2012-05-15

Polyamidoamine Dendrimer Nanoparticle Cytotoxicity, Oxidative Stress, Caspase Activation and Infammatory Response: Experimental Observation and Numerical Simulation

Sourav Prasanna Mukherjee
Dublin Institute of Technology, sourav.mukherjee@dit.ie

Hugh Byrne
Dublin Institute of Technology, Hugh.byrne@dit.ie

Recommended Citation

Mukherjee, S.P., Byrne, H.J., 2012. Polyamidoamine dendrimer nanoparticle cytotoxicity, oxidative stress, caspases activation and infammatory response: experimental observation and numerical simulation. Nanomedicine: Nanotechnology, Biology, and Medicine, 9, 202-211 (2013) doi:10.1016/j.nano.2012.05.002

ELSEVIER
Nanomedicine: Nanotechnology, Biology, and Medicine
xx (2012) xxx–xxx
nanomedicine
Nanotechnology, Biology, and Medicine
Original Article
nanomedjournal.com

Polyamidoamine dendrimer nanoparticle cytotoxicity, oxidative stress, caspase activation and inflammatory response: experimental observation and numerical simulation

Sourav Prasanna Mukherjee, PhD[a,*], Hugh J. Byrne, PhD[b]

[a]*Centre for Radiation and Environmental Science (RESC), Focas Research Institute, Dublin Institute of Technology, Dublin, Ireland*
[b]*Focas Research Institute, Dublin Institute of Technology, Dublin, Ireland*

Received 9 November 2011; accepted 7 May 2012

Abstract

Mechanisms underlying the in vitro cytotoxicity of Polyamidoamine nano-dendrimers in human keratinocytes are explored. Previous studies demonstrated a systematic, dendrimer-generation-dependent cytotoxicity, oxidative stress, and genotoxicity. The emerging picture is of dendrimer endocytosis, endosomal rupture and subsequent mitochondrial attack and cell death. To understand the underlying mechanisms, the evolution of reactive oxygen species, intracellular glutathione, caspase activation, mitochondrial membrane potential decay, and inflammatory responses have been examined. Early-stage responses are associated with endosomal encapsulation, later-stage with mitochondrial attack. In all cases, the magnitude and evolution of responses depend on dendrimer generation and dose. The early-stage response is modelled using a rate equation approach, qualitatively reproducing the time, dose and generation dependences, using only two variable parameters. The dependence of the response on the nanoparticle physicochemical properties can thus be separated from internal cellular parameters, and responses can be quantified in terms of rate constants rather than commonly employed effective concentrations.

Key words: Polyamidoamine Dendrimer; Molecular mechanism of cytotoxicity; Rate equation model; Numerical simulation

The rapid advance of nanotechnology has rendered it imperative that possible hazardous effects of nanomaterials on humans and the environment are elucidated. Nanoparticles (NPs) with different chemical composition and size have been shown to induce different levels of injury to cells and organisms, and thus a fundamental understanding of the mechanisms of their interaction is critical.[1] In vitro studies have demonstrated that the generation of intracellular reactive oxygen species (ROS) by NPs is a key to their toxicity by triggering different cell-death pathways, including cytokine[2] and caspase-activation[3] and nuclear-DNA damage.[4]

To elucidate the mechanisms underlying toxic responses and establish structure-activity-relationships, NPs of well-defined physicochemical properties that are systematically variable and elicit systematically variable cellular responses can play a key role. PAMAM dendrimers are widely explored, commercially available NPs of well-defined structure.[5-9] They have a 2-carbon ethylenediamine core with terminal amidoamines attached, yielding a highly branched radial structure having tertiary-amine branches and primary surface amino-groups. The diameter and number of surface amino-groups increases systematically with increasing generation.[5]

PAMAM dendrimers have been proposed for a range of biomedical applications, from MRI contrast agents,[10] to targeted delivery of drugs,[11] DNA,[12] and siRNA,[14] However, they have been reported to be toxic to mammalian cell lines[5-9] and aquatic species.[7] The polar surface amino groups impart an effective cationic charge, and endocytosis leads to oxidative-stress, mitochondrial and DNA damage, and ultimately apoptosis.[5-9] PAMAM dendrimers have also been reported to activate expression of different cytokines, such as tumor necrosis factor (TNF-α), interleukin-6 (IL-6), and macrophage inflammatory protein-2 (MIP-2), in a mouse macrophage cell line.[8] Previous studies have demonstrated the cytotoxicological responses to these species to vary systematically with increasing dendrimer generation and therefore number of surface amino groups.[5,6,8] A similar systematic response was observed for the generation of ROS, onset of apoptosis, and levels of DNA damage.[6] The mechanism of the toxic response has been at least partially elucidated, based on standard cytotoxicity assays including MTT, AB, and NR and microscopic co-localization studies.[6,15]

No conflict of interest was reported by the authors of this article.

*Corresponding author: RESC, Focas Research Institute, Dublin Institute of Technology, Dublin 8, Ireland.
E-mail address: sourav.mukherjee@dit.ie (S.P. Mukherjee).

1549-9634/$ – see front matter © 2012 Elsevier Inc. All rights reserved.
doi:10.1016/j.nano.2012.05.002

The mechanistic model which has emerged is one of endocytosis, oxidative stress, endosomal rupture through the proton-sponge effect, followed by mitochondrial damage and the onset of apoptosis.[6,16] The use of amine groups to induce endosomolytic behavior is a well-established strategy in drug delivery,[17] and the endosomolytic activity observed for PAMAM dendrimers is consistent with this. The cellular toxicity thus has primarily two phases; an early-stage, in which oxidative stress is primarily due to the presence of particles in endosomes, and a later stage, in which the particles migrate to the mitochondria, generating further oxidative-stress.[6,9] However, the toxicity of a specific NP to different cell lines can differ, due to the differences in intracellular constituent levels.[6] Understanding the metabolic pathways in the target cell, and their dose and time dependencies, is therefore critical to understanding the toxic responses in vitro, and ultimately in vivo.

In this study, the mechanism of PAMAM toxicity to the human keratinocyte, HaCaT, cell line is further explored. ROS production upon exposure to different PAMAM generations and doses is monitored as a function of time. Intracellular levels of the antioxidant glutathione (GSH), representative of the natural cellular antioxidant defense mechanisms, are also monitored. Changes in caspase-8 and caspase-3 activity, mitochondrial membrane potential (MMP) and TNF-α, IL-8 expression, over an exposure period of 24 hours are also explored. Based on the observations, potential underlying pathways for the early- and late-stage cellular responses are proposed.

The early-stage responses are visualized with the aid of a phenomenological rate-equation model, which qualitatively reproduces the generation and dose dependence of the sequence of events. It is highlighted that, although simplistic, such a rate-equation approach is a valuable tool in visualizing and elucidating cellular responses. It identifies response rates as critical parameters in determining toxicity and potentially a more reliable route towards quantitative structure-activity relationships than commonly employed cytotoxicological endpoints.

Methods

Commercially available PAMAM dendrimers of generation 4 (G4), 5 (G5) and 6 (G6) were used in this study. The nominal diameters of the PAMAM G4, G5, and G6 dendrimers are 4.5, 5.4, and 6.7 nm respectively.[5] Full physicochemical characterization has been reported.[5] All studies were performed using HaCaT cells. Assays were performed to evaluate ROS generation, GSH depletion, caspase-8 and 3 activation, mitochondrial membrane potential decay (MMPD), and TNF-α and IL-8 expression upon PAMAM exposure at different doses and time points. A detailed description of the materials used and experimental methods is given in the Supplementary Material available online at http://www.nanomedjournal.com.

Experimental results

ROS measurement

The generation of ROS shows a complex behavior as a function of time and dose for all PAMAM dendrimer generations, although the response is somewhat systematic as a function of generation. As a function of exposure time, a biphasic response is observed over a 24-hour time period at lower concentrations of PAMAM, as shown in Figure S1. At a fixed time point, the increase in ROS levels has been shown to increase monotonically with generation (Figure S1, *C*),[8] and when expressed in terms of molar concentration of surface NH_2 groups, the dose dependences of ROS for the different generations are overlaid.[13]

For PAMAM G6, an initial or early-stage maximum in ROS levels is observed after ~1 hour, for doses of 0.5 μM to 1.16 μM, whereas for higher doses (1.3 μM and 2.23 μM), the maximum is observed at ~0.5-hour exposure (Figure 1, *A*). At ~ 4 hours, exposure at all concentrations results in a reduction of the ROS levels below those of the control, whereas a later increase in the ROS levels is observed at ~24 hours for doses of 0.5 μM and 1 μM.

A similar behavior is observed for exposure to PAMAM G5, although the early-stage maximum for the lower doses has shifted toward the longer time of ~2 hours (Figure S1, *A*). This trend is continued for G4, all but the highest exposure concentration exhibiting a maximum response after ~3 hours (Figure S1, *B*). After ~24 hours, only the lowest dose exposure results in ROS levels above the control, all others being significantly quenched in comparison with the control levels.

At a concentration of 1μM, the maximum amount of ROS was produced after a ~ 24-hour exposure, the levels increasing with increasing generation of PAMAM (G4<G5<G6). Notably, this concentration is close to the EC_{50} of G5 and G6, as previously determined in HaCaT cells using MTT assay (Table S1), and at this concentration, increased lysosomal activity in comparison with control after ~24-hour exposure was also observed.[6] It was found that, at this concentration, in early stages after exposure (e.g., 1 hour), ROS levels increased linearly with number of surface amino groups per generation, as shown in Figure S1, *C*. With increasing doses, for all generations, after initial increase in ROS levels, the levels are seen to be reduced significantly below those of negative controls and do not recover over a 4-hour period.

ROS localization by CFM

Confocal fluorescence microscopy (CFM) demonstrates that early-increased (1 – 2 hour) levels of ROS localized in sacs/vesicles in cytosol (Figure S2, *A*), consistent with previous observations of early-stage trafficking of endocytosed PAMAM dendrimers in endosomes.[15] However, in the later stages (~24 hours), ROS are co-localized in the mitochondria (Figure S2, *B*), potentially indicating that they are generated through differing mechanisms.

GSH measurement

In control cells, intracellular GSH level increases approximately linearly as a function of time over 24 hours, as shown in Figure 1, *B*. Such a linear increase is commonly observed when studying in vitro cell cultures.[18,19] Upon exposure to PAMAM dendrimer solutions at a 1-μM concentration, initial linear increase in GSH levels follows the trend observed for control, but an abrupt deviation from the levels of controls is observed

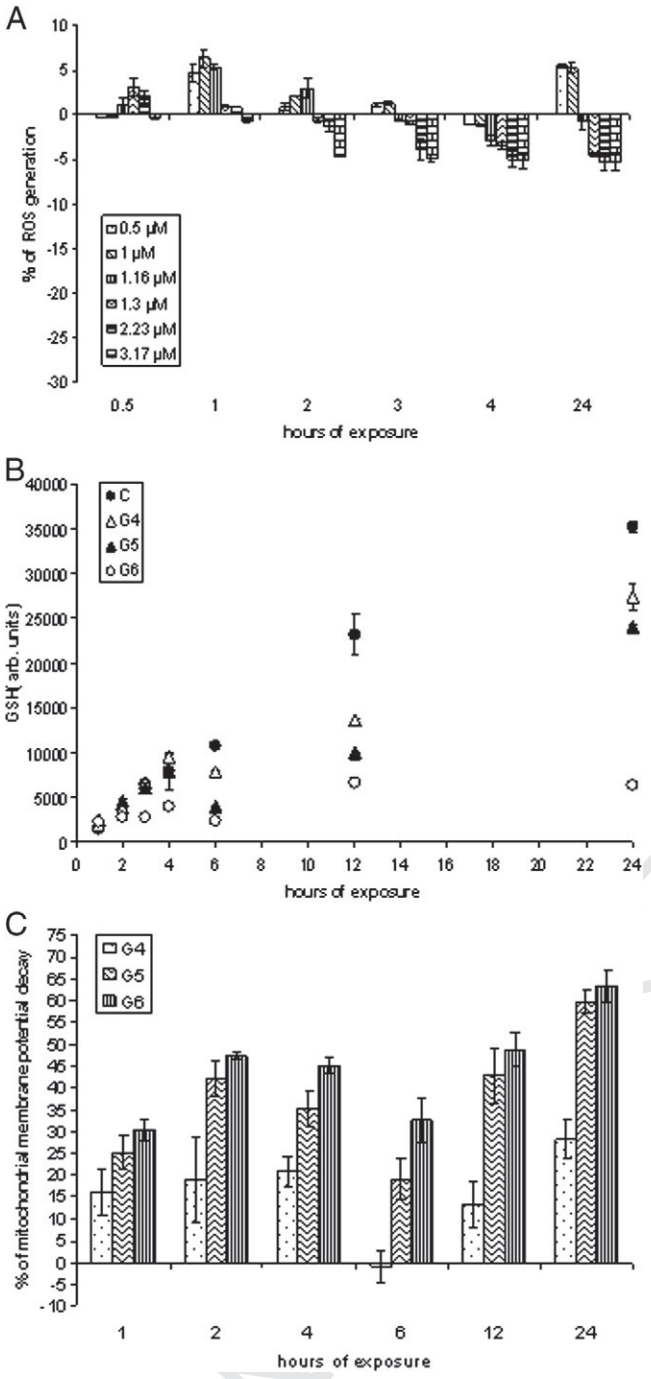

Figure 1. **(A)** ROS generation in HaCaT cells upon different concentrations of PAMAM G6 exposure. **(B)** GSH depletion upon 1 μM PAMAM G4, G5, G6 exposure in HaCaT cells as a function of exposure time. The y-axis shows the fluorescence intensity of the ThiolTracker Violet dye measured in the plate reader. The values are represented as arbitrary units (arb. units). **(C)** Mitochondrial membrane potential decay of HaCaT cells as a function of exposure time to 1 μM of PAMAM G4, G5, and G6.

within 1 – 5 hours. For G4, the deviation is observed after 4 hours, for G5 3 hours, and for G6 1 hour. Following these timepoints, the degree of reduction of the GSH levels is also seen to be systematic in dendrimer generation (G4<G5<G6).

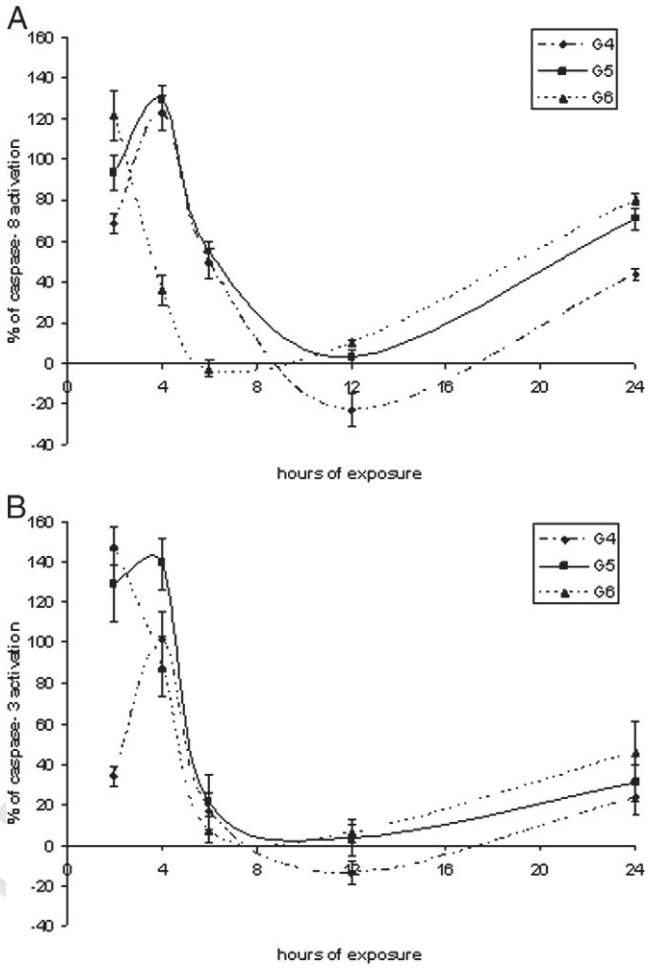

Figure 2. Expression of different caspases after exposure times of 1 μM PAMAM G4, G5 and G6- **(A)** caspase-8, **(B)** caspase-3.

Caspase-8 and -3 activity

The activity of caspase-8 and 3 was studied at different time points for 1-μM doses of PAMAM G4, G5, and G6. For both the caspases, a biphasic activity was observed (Figure 2). For PAMAM G4 and G5, an initial or early-stage maximum of caspase-8 levels was observed after ~4 hours' exposure, whereupon a minimum was observed before subsequent increase after 24 hours' exposure (Figure S3, *A*, S3, *B*). For G6, the early-stage maximum was found after ~2 hours' exposure (Figure S3*C*). Comparing the percentage increase of caspase-8 with control upon exposure to 1 μM for the different PAMAM generations after 24 hours, a systematic increase is observed (G4<G5<G6).

A similar behavior is observed for the time evolution of caspase-3 levels. For PAMAM G4 and G5, early-stage maximum were observed at ~4 hours' exposure and after an intermediate decrease, a late increase of caspase-3 activity was observed at 24 hours (Figure-S3, *A*, S3, *B*). For G6, early-stage increase of caspase-3 activity was observed at ~2 hours' exposure (Figure S3, *C*). Again, a systematic generation dependence of the percentage increase of caspase-3 levels in

comparison with control upon 1-μM exposure after 24 hours is observed (G4<G5<G6). Thus, although, in a similar way to the behaviour of ROS levels, the temporal evolution is complex, a clear systematic variation in the response with dendrimer generation is also evident.

Mitochondrial membrane potential decay

Upon exposure to 1-μM solutions of the respective PAMAM dendrimer generations over a 24-hour period, the percentage of mitochondrial membrane potential decay (MMPD), in comparison with controls, also shows a biphasic response, as shown in Figure 1, *C*. For all generations, the degree of MMPD increases initially within early stages of exposure. It then decreases to a minimum after ~ 6 – 7 hours of exposure, after which a further increase is observed up to 24 hours of exposure. The early-stage MMPD was observed after ~ 4 – 5 hours for G4 and ~ 2 – 3 hours for G5 and G6. At all time points, percentage of MMPD in comparison with control was seen to vary systematically with dendrimer generation (G4<G5<G6).

TNF-α and IL8 expression

An upregulation of TNF-α expression that is time, dose, and generation dependent was observed. For G4, the maximum amount of TNF-α was expressed at a concentration of 3.21 μM after ~6-hour exposure, as shown in Figure S4, *A*. For G5, the maximum amount of TNF-α expression was observed for 1 μM after ~ 4-hour exposure (Figure S4, *B*). For G6, the maximum amount of TNF-α is expressed at 1 μM after ~4-hour exposure (Figure S4, *C*). For a 1-μM dose, maximum percentage of TNF-α expression in comparison with the controls increases with increasing PAMAM generation (G4<G5<G6), although the maxima occur at different exposure times (Figure 3, *A*).

Over a 24-hour period, IL-8 expression shows a monotonic-increase for all doses, for all dendrimer generations, and the maximum response was observed after a 24-hour exposure. For G4, the maximum amount of IL-8 was expressed at 3.21 μM (Figure S5, *A*), for G5, at 1μM (Figure S5, *B*) and for G6 at 1 μM (Figure S5, *C*). The percentage of IL-8 expression in comparison with controls increases with increasing generation of PAMAM (G4<G5<G6), as shown for 1-μM dose in Figure 3, *B*.

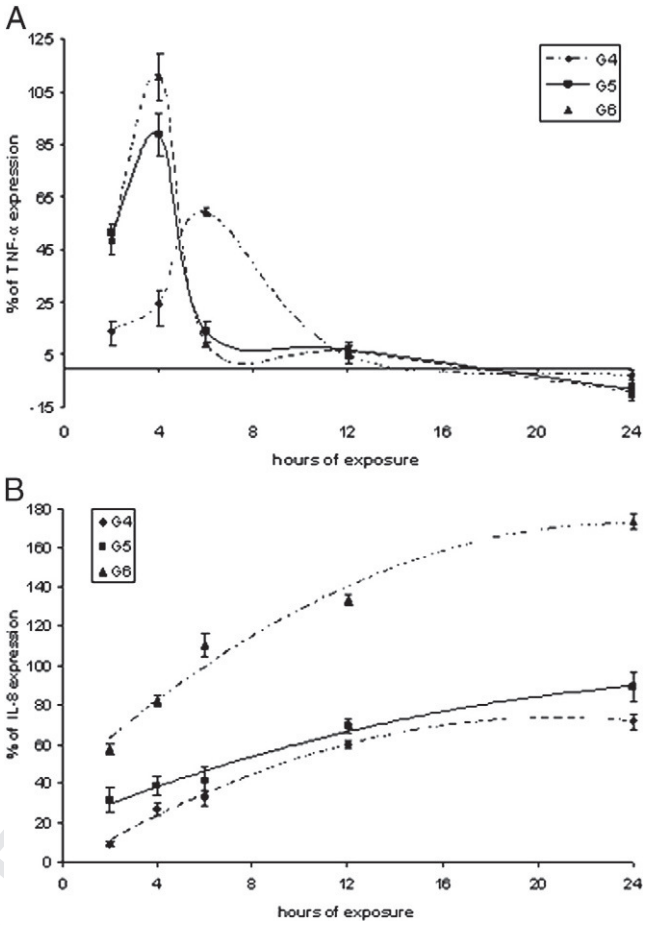

Figure 3. Inflammatory responses in HaCaT cells upon 1-μM exposures to all dendrimer generations for different time points **(A)** TNF-α, **(B)** IL-8.

Discussion and numerical simulation

The cellular responses upon exposure to PAMAM dendrimers are a complex function of generation, dose, and time. Figure 4 summarizes the time evolution of the cellular responses for the case of 1-μM exposure to the G6 dendrimer. The plot indicates a defined sequence of events, and the relative temporal evolutions of the different responses indicate some degree of interdependence of the responses.

Previous studies have demonstrated a two-phase response of cells to exposure to PAMAM dendrimers; early-stage localization in endosomes,[15] followed by a later-stage localization in mitochondria.[9] These two phases are well visualized in Figure S2, *A* and S2, *B*, whereby, at early stages, the ROS are primarily localized in smaller vesicles assumed to be endosomes, whereas after 24 hours, the ROS are mostly localized in the mitochondria. This two-stage process is further manifest in the time-dependent profile of the ROS levels at low doses, for all generations, as shown in Figure 1, *A*.

Key to the onset of the toxic response is the increase in ROS levels upon PAMAM exposure and the concomitant changes in intrinsic cellular antioxidant levels. As shown in Figure 1, *B*, a linear increase in cellular GSH levels is observed in control cells. Upon exposure to PAMAM dendrimers, a generation-dependent reduction in the rate of increase of GSH levels is observed. The degree and rate of reduction is generation dependent, associating the phenomenon with early-stage increase of ROS levels as a result of exposure.[20] It should be noted, upon careful inspection, that there is an apparent time lag between the onset of ROS and the deviation of the GSH levels from linearity. This lag is understandable in terms of differing experimental protocols used to monitor the respective responses. To monitor ROS levels, carboxy-H_2DCFDA dye was uploaded in the cells before particle exposure, whereupon ROS levels were measured after different exposure times. For the measurement of TNF-α, IL-8, and caspases, the cells were lysed immediately after exposure and so the exposure time was equal to the measurement time. To monitor GSH levels, however, cells were stained with ThiolTracker™ Violet for a period of ~30 minutes post

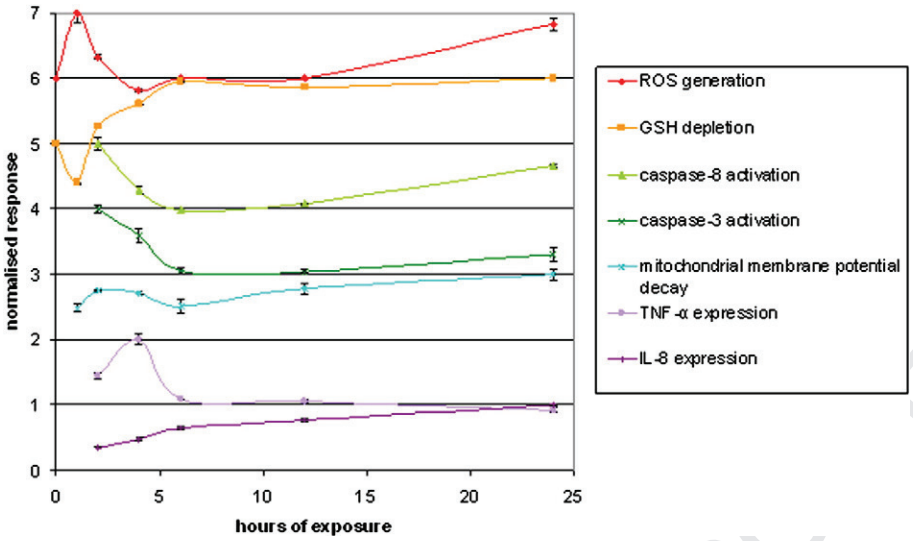

Figure 4. Representation of the different cellular responses as a function of time, for 1-μM exposure to PAMAM G6. For visual purposes, the responses from different assays have been normalized to 1 and different responses are offset by 1. The normalized responses are all in respect of negative controls, whereby the response for ROS represents percentage of ROS generation in comparison with control, GSH represents percentage of depletion in comparison with control; caspase-8, caspase- 3, TNF-α, and IL-8 represent percentage of expression in comparison with control; mitochondrial membrane potential decay represents percentage of MMPD in comparison with control.

exposure. Thus, including sample washing and preparation, there is a gap of 30 – 60 minutes from exposure time.

Although the results indicate systematic dependences of responses on dose and dendrimer generation, the four-dimensional response/dose/time/generation system is not easily visualized. To better visualize and elucidate the mechanisms of response, the system can be modeled using a simple phenomenological rate-equation model, similar to those commonly employed for modeling molecular photodynamics.[21] The particle dose and levels of ROS, GSH, etc., are described by populations, and changes in populations are governed by rate constants. The rate equations can be numerically integrated using an iterative Euler approach[22] to yield the temporal evolutions of the populations.

Salvati et al have demonstrated that the cellular uptake of polystyrene NPs occurs by endocytosis at a constant rate over a time period of 24 hours and that the rate is dose dependent.[23] In the case of PAMAM dendrimers, endocytotic process is assumed to be generation dependent, and thus the number of particles in the cells, N, increases as:

$$\frac{dN}{dt} = GK_{endo}D \qquad \text{Equation 1}$$

where K_{endo} is an endocytosis rate constant, G is a generation-dependent scaling factor, and D represents the dose. Once endocytosed, particles continuously generate ROS, build-up of ROS is counteracted by increased levels of GSH, and the interaction quenches both the levels of ROS and GSH. Thus:

$$\frac{dN_{ROS}}{dt} = NGK_{ROS} - K_q N_{ROS} N_{GSH} \qquad \text{Equation 2}$$

$$\frac{dN_{GSH}}{dt} = K_{GSH} - K_q N_{ROS} N_{GSH} \qquad \text{Equation 3}$$

The first term in Equation 2 is a generation- (G) and dose- (D) dependent term describing continuous ROS generation at a rate K_{ROS}. This rate is independent of dendrimer generation, but $DK_{ROS}G$ scales linearly with the number of surface amino groups per generation and dose. The second term describes the quenching of the ROS at a rate K_q, which depends on both ROS levels, N_{ROS}, and GSH levels, N_{GSH}. In Equation 3, the linear increase of the control levels of GSH, at a rate of K_{GSH}, is described by the first term, and the second term describes the quenching of the GSH levels. Thus, as a function of generation, for the same molar concentration, simply changing the parameter G for successive generations should reproduce the generation-dependent behaviors observed in Figures 1, *A* and 1, *B*, and, for a given dendrimer generation, changing D should similarly mimic the dose dependences of Figure 1, *A*.

Using a constant generation rate, however, the model predicts a monotonic increase in ROS levels over the exposure time, in contrast to early increase and decrease observed experimentally. If, however, the ROS population is constrained to saturate, a generation- and dose-dependent rise and fall is reproduced. To simulate such saturation, the rate of generation is proposed to be dependent on the number of ROS generated and thus time such that:

$$\frac{dK_{ROS}}{dt} = -K_{ROS} N_{ROS} \qquad \text{Equation 4}$$

Figure 5, *A* shows the predicted time and generation dependence of the rate of generation of ROS. Based on such a saturable ROS generation rate, Figure 5, *B* and 5, *C* show the

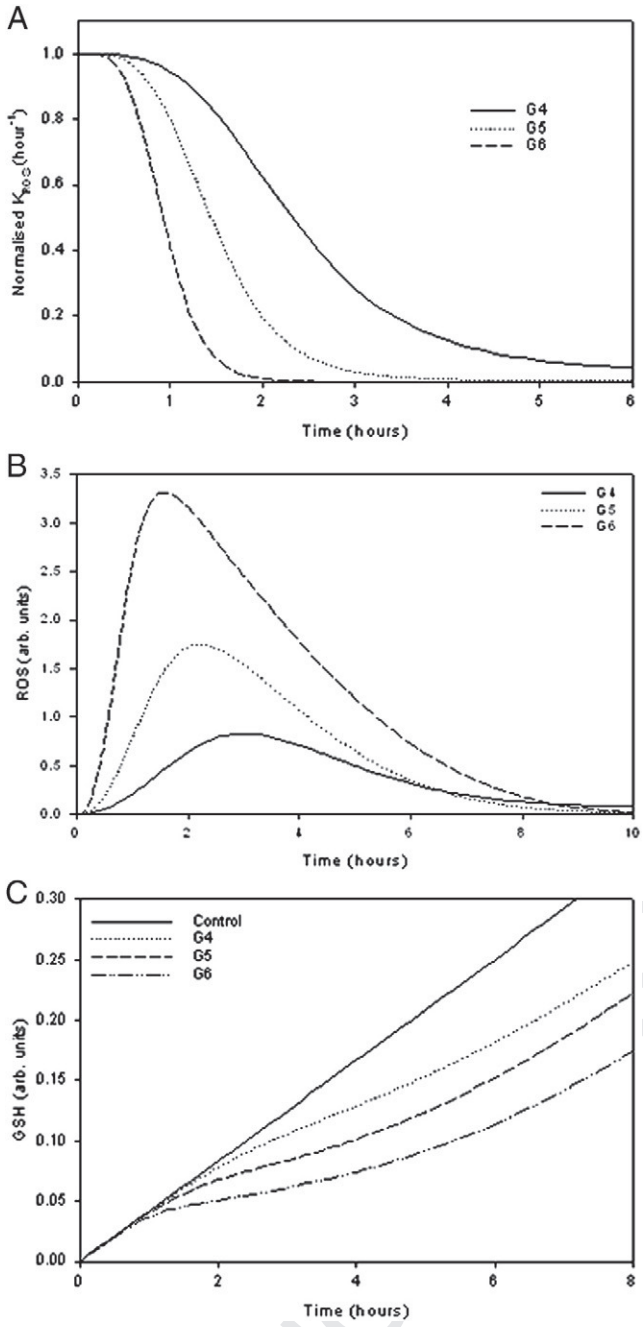

Figure 5. The simulated behaviors for all dendrimer generations of **(A)** the rate of ROS generation, K_{ROS}, **(B)** the levels of intracellular ROS, and **(C)** the levels of intracellular GSH as a function of time. In **(C)**, the solid line depicts the linear increase of GSH levels in negative controls.

simulated behaviors for the levels of intracellular ROS and GSH as a function of generation. For G4, maximum ROS levels are observed at ~3 hours, for G5 at ~2 hours, and for G6 at ~1.6 hours, in good agreement with experimental observations. Notably, however, the evolution curves of Figure 5, *B* are not as sharply varying with time as the behaviors observed experimentally in Figure 1, *A*. This is a result of the simplistic representation of the rate of generation of ROS in Equations (2-4). This is further manifest in the smooth departure of the levels of GSH from linearity in Figure 5, *C*, in comparison with rather abrupt behavior observed in Figure 1, *B*. The time delay between experimental ROS and GSH generation observed by comparing Figures 1, *A* and 1, *B* is further manifest here, as the modeled GSH follows the modeled increase in ROS levels. Because of the complexity of multiple processes leading to ROS generation and saturation, the simulation cannot therefore be considered to be a fit to the experimental data. Nevertheless, the simplistic approach qualitatively reproduces generation-dependent departure from linearity of the GSH levels in both extent and rate.

The simulations similarly faithfully predict an approximately linear dependence of the relative amounts of ROS on generation number, and therefore on number of surface amino groups for a fixed time and dose, as shown in Figure S6, *A* for the case of 1 hour of exposure of G6. At the 6-hour time point, however, a notably different behavior is observed, highlighting the importance of experimentally monitoring the full-time evolution of the response. Moreover, as the maxima shift in time as a function of dose and generation, at specific time points, complex dose dependences similar to those in Figure 1, *A*, can be reproduced, as shown in Figure S6, *B* for the cases of 1 hour, 1.5 hours and 2 hours of G6 exposure.

It should be noted that biphasic ROS generation is observed only at low doses in a generation-dependent fashion. At elevated doses, the levels of GSH are depleted such that the ROS levels are not quenched and no intermediate time-scale minimum in their levels is observed. In Figure 5, *C*, the generation dependence of this process is apparent in the prolonged timescales of GSH depletion, which further increase with increasing dose.

The activities of both caspase-8 and 3 upon 1-μM PAMAM exposure were also found to be biphasic over 24 hours for all generations (Figures 2, S3). The maximum percentages of early caspase-8 were activated after ~4 hours' exposure of G4 and G5, whereas those for G6 occurred after ~2 hours' exposure (Figure 2, *A*). The activity then decreased to, or below, the level of the control after ~12 hours for G4 and G5 and after ~6 hours for G6, before subsequently increasing to a maximum after 24 hours' exposure (Figure 2, *A*). Variations in activity of caspase-3 follow a trend similar to that of caspase-8 (Figure 2, *B*). In both cases, the activity profile and the percentage activity in comparison with control are dependent on generation.

In an attempt to understand the possible underlying response pathways, it is noted that apoptosis can be mediated through two major pathways, the death-receptor pathway (extrinsic)[24] and the mitochondrial pathway (intrinsic).[25] Notably, caspase-8 and 3 activations are seen to occur almost instantaneously after ROS generation, both in early and late stages. The observation of the early-stage maximum activation of caspase-8 before the maximum early-stage MMPD and activation of TNF-α indicates that caspase-8 activation in the current study is via the Fas/FasL mediated FADD pathway, independent of the TNF-α mediated FADD or mitochondrial pathway[26] (Figure 4). Previously it was also shown that intracellular ROS mediates Fas-ligation that leads to caspase-8 and 3 activation.[27] It is therefore proposed that activation of early caspase-8 and 3 is mediated via extrinsic FasL mediated Fas-signaling pathway.[27,28] Caspase-8 activation acts as an

upstream process for caspase-3 activation by activating pro-caspase-3.[29] FADD pathway can be naturally inactivated by caspase-8-like inhibitory protein (cFLIP)[30,31] or can be inhibited by the inhibitors of apoptosis proteins (IAPs), for example X-linked inhibitor of apoptosis protein (XIAP).[32,33] Such mechanisms can potentially decrease the activity of caspase-8 and 3 after its early activation (Figures 2, S3).

The activation of caspase-8 by intrinsic mitochondrial pathway, which is independent of the classical FADD pathway, is also well known.[34,35] Through this pathway, caspase-8 can be activated either via mitochondrial p38-MAPK or mitogen- and stress-response kinase 1 (MSK1), which are sequentially activated upon mitochondrial oxidative-stress (Mchichi et al, 2007). The second-phase of caspase-activation follows the second-phase of ROS, generated in the mitochondria, thereby causing mitochondrial oxidative-stress. Therefore, its activation could potentially occur through the mitochondrial p38-MAPK or MSK1 pathway.

The expression of TNF-α, a pro-inflammatory cytokine, can also be activated by p38-MAPK and other MAPKs upon oxidative stress.[36] NPs have been shown to upregulate TNF-α and CXCL8 via ROS and MAPK activation.[37] TNF-α activation in turn activates the expression of the chemokine IL8.[38] It has also been reported that TNF-α downregulates FasL expression in the vascular endothelial cells.[39] Therefore, sequential TNF-α and IL8 expressions following early-stage maximum in ROS generation caspase activation, and MMPD is consistent with its activation by a MAPK pathway. TNF-α activation before the second-phase of caspase activation possibly activates Smac/Diablo, which inhibit IAPs,[40] resulting in the second phase of caspase activity with prolonged exposure time.

The mitochondrial membrane potential study reveals that the decay rapidly follows the caspase activation, in both early and later stages, with a delay of ~ 45 minutes to 1 hour (Figures 2 and 1, *C*). This delay comes in part from the staining of the cells with rhodamine-123 for measuring mitochondrial membrane potential after the exposure time point, whereas in caspase study the cells were lysed immediately after exposure. Therefore, caspase activation, which is an instantaneous effect of ROS generation, probably via Fas pathway, results in rapid decay of MMP.[28] The extent of MMPD and the time evolution is generation dependent (Figure 1, *C*). The biphasic response is consistent with the model of early-stage ROS generation by particles in subcellular vesicles, most likely endosomes, which cause oxidative stress to the mitochondria, followed by endosomal release and localization of the dendrimer particles in the mitochondria, leading to cell death via the mitochondrial injury pathway,[41] generating further ROS as a result.[41,9] The decrease in MMPD after the early-stage increase could be due to the effects of mitochondrial chaperones, e.g., prohibitin, which elevate the synthesis of ATP and stabilize MMP, delaying the onset of apoptosis.[42]

The inflammatory study indicates a subsequent sequential activation of TNF-α and IL-8. The maximum TNF-α expression was observed after ~6 hours' exposure at 3.21 μM for G4 and after ~4 hours' exposure at 1 μM for G5 and G6 (Figure 3, *A*). Having reached the maximum, the expression is seen to decrease with exposure time to levels less than control. The expression of IL-8 increases monotonically with exposure time to a maximum at 24 hours' exposure at 3.21 μM for G4, and 1 μM for G5 and G6 (Figure 3, *B*). Above and below these concentrations, the expression of TNF-α and IL-8 decreases. Notably, these concentrations are also the EC_{50} values obtained from the dose response from MTT assay in HaCaT cells[5] (Table S1). The maximum percentage of increase of TNF-α and IL-8 expression was also seen to increase with increasing generation of PAMAM dendrimer, and therefore number of surface amino groups.

It is notable that TNF-α activation is only observed in the early stages and does not follow the biphasic evolution of ROS and caspase activation and MMPD. In the early stages, the NPs are located in vesicles, proposed to be endosomes, and thus oxidative stress is generated external to the mitochondria. At the later stages, dendrimer NPs and generation of ROS have been located in the mitochondria.[9,6] Although derived from the mitochondria, it has been demonstrated that acute, internal stress can suppress the expression of pro-inflammatory cytokines, such as TNF-α,[43] without affecting IL-8 expression.[44] Similarly, PAMAM generates acute stress when incorporated into mitochondria (24 hours)[6] and the second phase of TNF-α expression is not observed in our study.

In the first phase of evolution, the rate-equation model can be simply extended to include the ROS-dependent activation of caspases, and subsequent MMPD and generation of TNF-α and IL8, and thus visualize the generation and dose dependences, as described in the Supplementary Material. Figure 6, *A–C* illustrates the time evolution of the process as well as generation-dependent behavior predicted by the model, simply by changing the parameter G in Equations (1) and (2). All rates are kept constant and the differing rates of evolution of subsequent stages are the result of the early-stage generation- (or dose-) dependent increase in ROS levels. For example, maximum TNF-α expression is predicted for G4 at 5.1 hours, for G5 at 4.4 hours and for G6 at 4 hours. Although the experimental time intervals do not differentiate the maxima for G5 and G6, the model predicts a sequence of activation of G6<G5<G4. Furthermore, although the magnitudes of responses are normalized to the maximum for graphical representation, at each step in the cascade, the generation dependence of G6>G5>G4 is also reproduced faithfully, as shown by the approximately linear dependence of the maximum levels of TNF-α, as a function of number of surface amino-groups per dendrimer generation in Figure S7.

In all cases, only the early stage of the cellular responses has been modeled. This stage is proposed to originate from initial endocytosis of the particles and encapsulation in endosomes. ROS is most likely generated via the proton-pump mechanism, resulting in depletion of GSH and other antioxidants and the onset of caspase activation, MMPD, and inflammatory responses via TNF-α activation. The second phase appears to be spatially distinct, in that it is associated with localization of dendrimer NPs and ROS generation in the mitochondria. Although the second phase is not modeled here, a similar rate-equation approach could be employed to simulate the responses, their time evolution and dependences on dose and dendrimer generation. A more complete understanding of

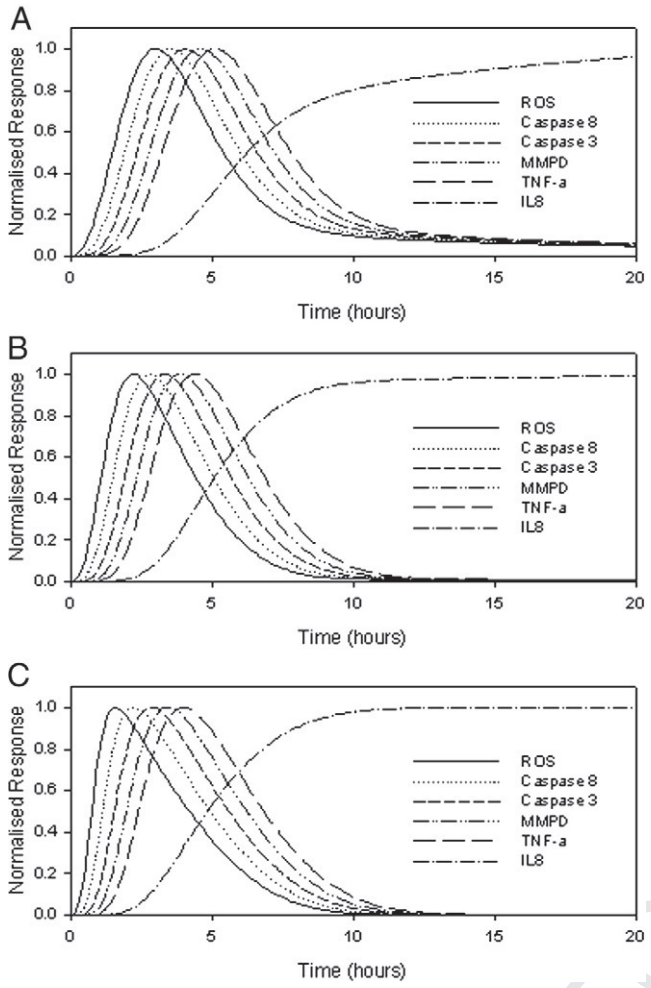

Figure 6. Illustration of the generation dependent behavior for **(A)** G4, **(B)** G5, and **(C)** G6, in terms of normalized ROS generation, MMPD and TNF-α and IL8 expression, predicted by the model, simply by changing the parameter G in Equation (2).

generation and dose dependence of the process of endosomal rupture, particle migration to and uptake by the mitochondria, and recovery of intracellular antioxidant levels would be required. Between the two phases, such phenomena as the quenching of ROS levels to below those of controls, the recovery of antioxidant levels, and migration of antioxidants to localised subcellular sites should be considered. Nevertheless, the phenomenological model is readily adaptable to include more complex phenomena, simply by adding additional terms to the rate equations (Equation S1–S5).

The overall mechanism that can be postulated from the cellular responses is diagrammatically represented in Figure S8. PAMAM dendrimers enter the cells by endosomal uptake or by rupture of the plasma membrane.[15,6,45] Initial oxidative stress results from early-stage ROS generation whereas the dendrimers are encapsulated in early-stage subcellular vesicles, most likely endosomes.[6] The generation dependence of the ROS generation rate and yield point to the reactive NH_2 surface groups as the origin of oxidative stress. Intracellular antioxidants result in a quenching of early-stage ROS and are themselves quenched by the action.[46] The study of GSH levels and their time evolution, as an example of intracellular antioxidants, highlights the importance of intracellular defense mechanisms, and potentially points to a source of differentiation of different cellular responses to NP exposure. The ROS probably play a pivotal role in the possible FasL/Fas mediated activation of caspase-8 which further activates caspase-3, leading to the initial MMPD. Maximum TNF-α expression after early-stage maximum ROS, caspase-8 and 3 activities and MMPD suggests TNF-α activation by mitochondrial pathway. TNF-α subsequently induces IL-8 expression and therefore its expression gradually increases with exposure time. After reduction of early-stage ROS, it is proposed that the action of different caspase inhibitor proteins results in reduction of caspase-8 and 3 activities and MMP similarly recovers, possibly through the action of mitochondrial chaperones. In the second phase, PAMAM dendrimers rupture the endosomes by so-called "proton-sponge effect" and are released into the cytosol and interact directly with other cellular organelles. After ~16 hours they have been located in the mitochondria,[9] whereupon the oxidative stress is increased, resulting in further MMPD. No further TNF-α expression is observed, but a second phase of activation of caspases is observed, which is possibly through the mitochondrial pathway. The sequential and potentially independent pathways of caspase activations that are associated with the early and late stage of ROS generation can be understood by further studies of the activation of Fas and mitochondrial p38MAPK or MSK1. The potential role of IAPs and cFLIP in the inhibition of caspase-8 and 3 after their early-stage activation and the contribution of Smac/Diablo activation profile should also be studied for further elucidation of the biphasic caspase activation. Following the activation of these different cell-death pathways and the activation of caspases, the cell enters apoptosis, its nuclear DNA undergoes fragmentation, and finally it dies.[6]

Although simplistic at this stage, the numerical modeling approach enables a visualization of the complex generation, dose and time dependences of the cellular responses. A fundamental understanding of in vitro cytological responses is becoming increasingly important, given the implications of EU Directive 2010/63/EU on reduction, replacement, and refinement of animal models for scientific experimentation. Consideration of the responses in terms of rate equations elucidates their sequence, interdependencies, and relative magnitudes. It is a potential route towards quantifying nanotoxicological responses in terms of response rates that are determined by NP properties and cellular and even cell-line-dependent parameters, independently. The overall cytotoxicological response, as frequently monitored by classic cytotoxicological assays and expressed, for example, as an EC_{50}, is a convolution of a cascade of events, which can potentially be better expressed as response rates that can be defined per NP and cellular system.

A nonlinear response and saturation are required to reproduce the experimental observations, but the origin and mathematical form of this nonlinearity and saturation requires clarification. In cytotoxicity, dose dependences are commonly empirically represented by the Hill function,[47] but this is not

easily represented in a form that indicates the rates of contributing processes.[48] In pharmacokinetics, it is simply acknowledged that to account for a nonlinear response to a linear dose, at least one of the intermediate stages must be nonlinear.[49]

The endocytotic process is assumed to be linearly dependent on dose, but a low-dose exposure of many cells to few NPs is most likely significantly different from one in which there are many particles per cell, and ultimately the capacity of a single cell to endocytose NPs must be limited. In the simplistic treatment presented here, no changes to cell population due to cell proliferation or death have been included. The doubling time for HaCaT cells is 23 hours.[50] The Alamar Blue assay shows that, upon exposure to 1μM PAMAM G6 for 24 hours, the percentage cytotoxicity in comparison with control was 28% (data not shown). Therefore, it is predictable that after 6 hours' exposure the effect of 1μM G6 on HaCaT cell proliferation and viability was not significant.

Notably, the dose dependence of ROS generation is nonlinear and potentially originates in its time evolution. However, although the model demonstrates how a complex dose dependence can arise, the results are by no means a fit with the experimental data, and further work utilizing model NP systems is required to accurately predict the dose dependence. Ultimately, however, such a rate-equation model may provide the basis for quantification of NP toxicity and cellular susceptibility, and thus quantitative structure-activity relationships.

Appendix A. Supplementary data

Supplementary data to this article can be found online at http://dx.doi.org/10.1016/j.nano.2012.05.002.

References

1. Stone V, Donaldson K. Nanotoxicology: signs of stress. *Nat Nanotechnol* 2006;**1**:23-4.
2. Brown DM, Donaldson K, Borm PJ, Schins RP, Dehnhardt M, Gilmour P, et al. Calcium and ROS-mediated activation of transcription factors and TNF- a cytokine gene expression in macrophages exposed to ultrafine particles. *Am J Physiol Lung Cell Mol Physiol* 2004;**286**:L344-53.
3. Kim BM, Choi YJ, Han Y, Yun Y-S, Hong SH. N, N-dimethyl phytosphingosine induces caspase-8-dependent cytochrome c release and apoptosis through ROS generation in human leukemia cells. *Toxicol Appl Pharmacol* 2009;**239**:87-97.
4. Cooke MC, Evans MD, Dizdaroglu M, Lunec J. Oxidative DNA damage: mechanisms, mutation, and disease. *The FASEB Journal* 2003; **17**:1195-214.
5. Mukherjee SP, Davoren M, Byrne HJ. In vitro mammalian cytotoxicological study of PAMAM dendrimers –Towards quantitative structure activity relationships. *Toxicol In Vitro* 2010;**24**(1):1169-77.
6. Mukherjee SP, Lyng FM, Garcia A, Davoren M, Byrne HJ. Mechanistic studies of in vitro cytotoxicity of Poly(amidoamine) dendrimers in mammalian cells. *Toxicol Appl Pharmacol* 2010;**248**(3):259-68.
7. Naha PC, Davoren M, Casey A, Byrne HJ. An ecotoxicological study of *Poly(amidoamine)* dendrimers - toward quantitative structure activity relationships. *Environ Sci Technol* 2009;**43**:6864-9.
8. Naha PC, Davoren M, Lyng FM, Byrne HJ. Reactive oxygen species (ROS) induced cytokine production and cytotoxicity of PAMAM dendrimers in J774A.1 cells. *Toxicol Appl Pharmacol* 2010;**246**:91-9.
9. Lee JH, Cha KE, Kim MS, Hong HW, Chung DJ, Ryu G, et al. Nanosized polyamidoamine (PAMAM) dendrimer-induced apoptosis mediated by mitochondrial dysfunction. *Toxicol Lett* 2009;**190**:202-7.
10. Bourne MW, Margerun L, Hylton N, Campion B, Lai JJ, Derugin N, et al. Evaluation of the effects of intravascular MR contrast media (gadolinium dendrimer) on 3D time of flight magnetic resonance angiography of the body. *J Magn Reson Imaging* 1996;**6**:305-10.
11. Twyman LJ, Beezer AE, Esfand R, Hardy MJ, Mitchell JC. The synthesis of water soluble dendrimers, and their application as possible drug delivery systems. *Tetrahedron Lett* 1999;**40**:1743-6.
12. Guillot-Nieckowski M, Eisler S, Diederich F. Dendritic vectors for gene transfection. *New J Chem* 2007;**31**:1111-27.
13. Naha PC. Eco and in vitro mammalian toxicological assessment of polymeric nanomaterials, PhD thesis, DIT, 2011.
14. Zhou J, Wu J, Hafdi N, Behr JP, Erbacher P, Peng L. PAMAM dendrimers for efficient siRNA delivery and potent gene silencing. *Chem Commun (Camb)* 2006;**22**:2362-4.
15. Kitchens KM, Foraker AB, Kolhatkar RB, Swaan PW, Ghandehari H. Endocytosis and interaction of Poly (amidoamine) dendrimers with Caco-2 Cells. *Pharmaceut Res* 2007;**24**:2138-45.
16. Nel AE, Mädler L, Velegol D, Xia T, Hoek EMV, Somasundaran P, et al. Understanding biophysicochemical interactions at the nano–bio interface. *Nat Mater* 2009;**8**:543-57.
17. Watson P, Jones AT, Stephens DJ. Intracellular trafficking pathways and drug delivery: fluorescence imaging of living and fixed cells. *Adv Drug Deliv Rev* 2005;**57**:43-61.
18. Bajt ML, Knight TR, Lemasters JJ, Jaeschke H. Acetaminophen-induced oxidant stress and cell injury in cultured mouse hepatocytes: protection by *N*-acetyl cysteine. *Toxicol Sci* 2004;**80**:343-9.
19. Ding W-X, Shen H-M, Ong C-N. Microcystic cyanobacteria extract induces cytoskeletal disruption and intracellular glutathione alteration in hepatocytes. *Environ Health Perspect* 2000;**108**:605-9.
20. Ossola JO, Tomaro ML. Heme oxygenase induction by UVA radiation. A response to oxidative stress in rat liver. *Int J Biochem Cell Biol* 1998;**30**:285-92.
21. Penzkofer A, Blau W. Theoretic analysis of S1-state lifetime measurements of dyes with picoseconds laser pulses. *Opt Quant Electron* 1983;**15**:325-47.
22. Ascher UM, Petzold LR. Computer methods for ordinary differential equations and differential-algebraic equations. SIAM, 1998; ISBN 0898714125.
23. Salvati A, Aberg C, Dos Santos T, Varela J, Pinto P, Lynch I, et al. Experimental and theoretical comparison of intracellular import of polymeric nanoparticles and small molecules: toward models of uptake kinetics. *Nanomedicine* 2011, http://dx.doi.org/10.1016/j.nano.2011.03.005.
24. Wajant H. The Fas signaling pathway: more than a paradigm. *Science* 2002;**296**:1635-6.
25. Desagher S, Martinou JC. Mitochondria as the central control point of apoptosis. *Trends Cell Biol* 2000;**10**:369-77.
26. Gu Q, Wang JD, Xia HHX, Lin MCM, He H, Zou B, et al. Activation of the caspase-8/Bid and Bax pathways in aspirin-induced apoptosis in gastric cancer. *Carcinogenesis* 2005;**26**:541-6.
27. Anathy V, Aesif SW, Guala AS, Havermans M, Reynaert NL, Ho Y-S, et al. Redox amplifi cation of apoptosis by caspase-dependent cleavage of glutaredoxin 1 and S-glutathionylation of Fas. *JCB* 2009;**184**: 241-52.
28. Uriarte SM, Joshi-Barve S, Song Z, Sahoo R, Gobejishvili L, Jala VR, et al. Akt inhibition upregulates FasL, downregulates c-FLIP$_s$ and induces caspase-8-dependent cell death in Jurkat T lymphocytes. *Cell Death Differ* 2005;**12**:233-42.
29. Stennicke HR, Jürgensmeier JM, Shin H, Deveraux Q, Wolf BB, Yang X, et al. Pro-caspase-3 is a major physiologic target of caspase-8. *J Biol Chem* 1998;**273**:27084-90.
30. Wang L, Du F, Wang X. TNF-alpha induces two distinct caspase-8 activation pathways. *Cell* 2008;**133**:693-703.

31. Jiang Z, Clemens PR. Cellular caspase-8-like inhibitory protein (cFLIP) prevents inhibition of muscle cell differentiation induced by cancer cells. *FASEB J* 2006;**20**:2570-2.
32. Le Blanc AC. Natural cellular inhibitors of caspases. *Prog Neuropsychopharmacol Biol Psychiatry* 2003;**27**:215-29.
33. Bratton SB, Lewis J, Butterworth M, Duckett CS, Cohen GM. XIAP inhibition of caspase-3 preserves its association with the Apaf-1 apoptosome and prevents CD95- and Bax-induced apoptosis. *Cell Death Differ* 2002;**9**:881-92.
34. Mchichi BE, Hadji A, Vazquez A, Leca G. p38 MAPK and MSK1 mediate caspase-8 activation in manganese-induced mitochondria-dependent cell death. *Cell Death Differ* 2007;**14**:1826-36.
35. Schrantz N, Bourgeade MF, Mouhamad S, Leca G, Sharma S, Vazquez A. p38-mediated regulation of an Fas-associated death domain protein-independent pathway leading to caspase-8 activation during TGFbeta-induced apoptosis in human Burkitt lymphoma B cells BL41. *Mol Biol Cell* 2001;**12**:3139-51.
36. Ke Q, Li J, Ding J, Ding M, Wang L, Liu B, et al. Essential role of ROS-mediated NFAT activation in TNF-α induction by crystalline silica exposure. *Am J Physiol Lung Cell Mol Physiol* 2006;**291**:L257-64.
37. Lee H-M, Shin D-M, Song H-M, Yuk J-M, Lee Z-W, Lee S-H, et al. Nanoparticles up-regulate tumor necrosis factor-α and CXCL8 *via* reactive oxygen species and mitogen-activated protein kinase activation. *Toxicol Appl Pharma* 2009;**238**:160-9.
38. Zhao R, Chen X, Yao Q, Chen C. TNF-α induces interleukin-8 and endothelin-1 expression in human endothelial cells with different redox pathways. *Mol Cell Biol Res Commun* 2005;**327**:985-92.
39. Sata M, Walsh K. TNFα regulation of Fas ligand expression on the vascular endothelium modulates leukocyte extravasation. *Nat Med* 1998;**4**:415-20.
40. Shiozaki EN, Shi Y. Caspases, IAPs and Smac/DIABLO: mechanisms from structural biology. *Trends Biochem Sci* 2004;**29**:486-94.
41. Xia T, Kovochich M, Brant J, Hotze M, Sempf J, Oberley T, et al. Comparison of the abilities of ambient and manufactured nanoparticles to induce cellular toxicity according to an oxidative stress paradigm. *Nano Lett* 2006;**6**:1794-807.
42. Liu X-H, Ren Z, Zhan R, Wang X-X, Wang X-M, Zhang Z-Q, et al. Prohibitin protects against oxidative stress-induced cell injury in cultured neonatal cardiomyocyte. *Cell Stress Chaperones* 2009;**14**:311-9.
43. Connor TJ, Brewer C, Kelly JP, Harkin A. Acute stress suppresses pro-inflammatory cytokines TNF-alpha and IL-1 beta independent of a catecholamine-driven increase in IL-10 production. *J Neuroimmunol* 2005;**159**:119-28.
44. Zhang Z, Cork J, Ye P, Lei D, Schwarzenberger PO, Summer WR, et al. Inhibition of TNF-alpha processing and TACE-mediated ectodomain shedding by ethanol. *J Leukoc Biol* 2000;**67**:856-62.
45. Hong S, Leroueil PR, Janus EK, Peters JL, Kober M-M, Islam MT, et al. Interaction of polycationic polymers with supported lipid bilayers and cells: nanoscale hole formation and enhanced membrane permeability. *Bioconjug Chem* 2006;**17**:728-34.
46. Zeisel SH. Antioxidants suppress apoptosis. *Am Soc Nutrit Sci J Nutr* 2004;**134**:3179S-80S.
47. Hill A. The possible effects of the aggregation of the molecules of haemoglobin on its disociation curves. *J Physiol (Lond)* 1910;**40**:4-8.
48. Sorribas A, Hernández-Bermejo B, Vilaprinyo E, Alves R. Cooperativity and saturation in biochemical networks: a saturable formalism using-taylor series approximations. *Biotechnol Bioeng* 2007;**97**:1259-77.
49. Black JW, Leff P. Operational models of pharmacological agonism. *Proc R Soc Lond B Biol Sci* 1983;**220**:141-62.
50. Boukamp P, Petrussevska RT, Breitkreutz D, Hornung J, Markham A, Fusenig NE. Normal human keratinization in a spontaneously immortalized aneuploid human keratinocyte cell line. *J Cell Biol* 1988;**106**: 761-71.

ELSEVIER

Nanomedicine: Nanotechnology, Biology, and Medicine
xx (2012) xxx

nanomedjournal.com

Graphical Abstract

Nanomedicine: Nanotechnology, Biology, and Medicine xx (2012) xxx

Polyamidoamine dendrimer nanoparticle cytotoxicity, oxidative stress, caspase activation and inflammatory response: experimental observation and numerical simulation

Sourav Prasanna Mukherjee, PhD [a,*], Hugh J. Byrne, PhD [b]

[a] *Centre for Radiation and Environmental Science (RESC), Focas Research Institute, Dublin Institute of Technology, Dublin, Ireland*
[b] *Focas Research Institute, Dublin Institute of Technology, Dublin, Ireland*

Structural dependence of cytotoxic responses to PAMAM dendrimers derive from ROS generation and resultant cascades can be visualized and simulated mathematically.

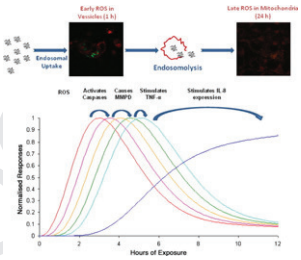

Supplementary Material